

Date of publication xxxx 00, 0000, date of current version xxxx 00, 0000.

Digital Object Identifier 10.1109/ACCESS.2019.Doi Number

Segmentation Guided Registration for 3D Spectral-domain Optical Coherence Tomography Images

LINGJIAO PAN,^{1,3} LILING GUAN,¹ and XINJIAN CHEN^{1,2*}, (Member, IEEE)

¹ The School of Electronic and Information Engineering, Soochow University, Suzhou, 215006, China

² The State Key Laboratory of Radiation Medicine and Protection, School of Radiation Medicine and Protection, Soochow University, Suzhou, 215006, China

³ The School of Electrical and Information Engineering, Jiangsu University of Technology, Changzhou, 213001, China

Corresponding author: Xinjian Chen. (xjchen@suda.edu.cn).

This work was supported in part by the National Nature Science Foundation of China for Excellent Young Scholars under 61622114, in part by the National Natural Science Foundation of China under Grant 81401472, 81371629, in part by the Natural Science Foundation of the Higher Education Institutions of Jiangsu Province under Grant 17KJB510015, in part by Collaborative Innovation Center of IoT Industrialization and Intelligent Production, Minjiang University under Grant IIC1702, and in part by the Changzhou Social Development Foundation under Grant CE20165021.

ABSTRACT Medical image registration can be used for combining information from multiple imaging modalities, monitoring changes in size, shape or image intensity over time intervals. However, the development of such technique can be challenging for 3D spectral-domain optical coherence tomography (SD-OCT) imaging, because SD-OCT image is inherently noisy and its high resolution leads to high complexity of non-rigid registration. In this paper, a new segmentation guided approach is reported for registration of retinal OCT data. The proposed method models the 3D registration as a two-stage registration including x-y direction registration and z direction registration. In x-y direction registration, the vessel maps of OCT projection images between the template and the subject are registered to find out x-y direction displacement. The multi-scale vessel enhancement filter and morphological thinning methods are used to extract the vessel maps from the projection image of 3D OCT scans. And then x-y direction displacement is estimated by matching Speeded-Up Robust Features of the vessel maps. In z direction registration, using the tissue map instead of the original intensity image, A-scans are aligned to get the local displacements in z direction. The proposed method was evaluated on 45 longitudinal retinal OCT scans from 15 subjects. Experimental results show that the proposed method is accurate and very efficient.

INDEX TERMS Medical image, image registration, non-rigid registration, spectral-domain optical coherence tomography (SD-OCT), Speeded-Up Robust Features (SURF), graph cut.

I. INTRODUCTION

The recent introduction of next generation spectral-domain optical coherence tomography (SD-OCT) has become increasingly important in detection and investigation of retinal related diseases [1-4]. 3D SD-OCT imaging technique is a noninvasive and non-contact imaging modality for biological tissues. It has been widely used for investigating retinal pathology since it can provide high resolution information of the retina. The principle of OCT is the estimation of the depth at which a specific backscatter originated by measuring its time of flight [5]. As shown in Fig. 1, the light is split into two beams by a beam splitter. One beam reflected from the retinal tissue is called the

sample arm and another beam reflected from the reference mirror is the reference arm. The interferogram energy between the sample arm and the reference arm is converted into image intensities with CCD or a photo sensor. A depth scan which is called A-scan is created from the interferogram intensities. For 3D imaging, SD-OCT device move the illuminating beam across the retina. By acquiring a series of A-scans in a raster scanning pattern, the cross sectional slicer B-scans are generated. Composing successive B-scans yields a 3D SD-OCT image of retina. Fig. 2 shows a 3D SD-OCT scan of retina which consists of B-scan slices. Each B-scan slice consists of A-scans.

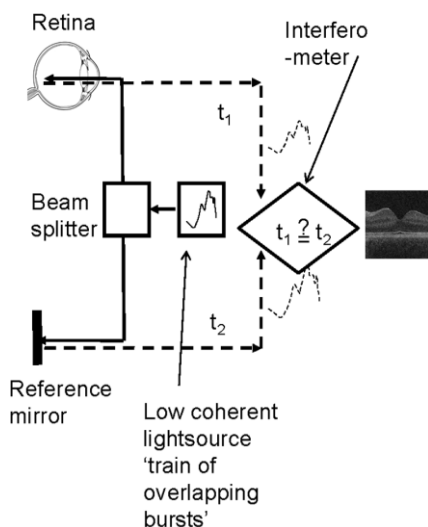


FIGURE 1. Schematic diagram of OCT image formation (cited from Ref. [5]).

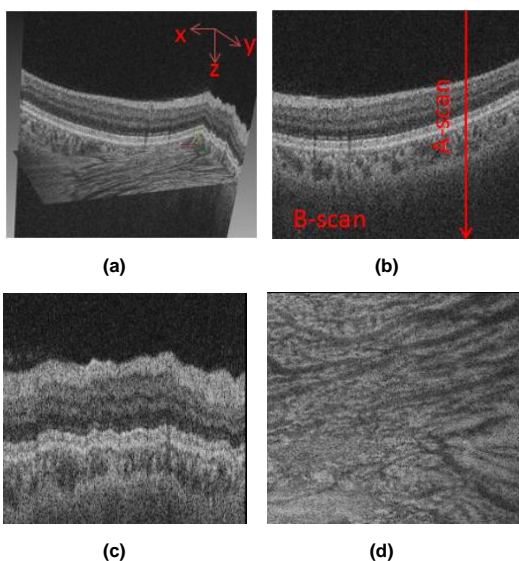


FIGURE 2. Example of a 3D SD-OCT scan of retina. All images have been resized for better display. (a) 3D view. (b) x-z view (B-scan). (c) y-z view. (d) Projection image.

Medical image registration has been a hot research topic over a decade. It has a wide range of clinical and research applications including combining information from multiple imaging modalities, monitoring changes in size, shape or image intensity over time intervals and so on [6-10]. To achieve a comprehensive description of retinal morphology and disease progression, diverse retinal images acquired by different or the same modalities at different time instants must be registered. Retinal registration can be divided into three categories: 1) fundus-fundus registration, which is useful to expand the effective field of view and analyze changes over time [11]; 2) fundus-OCT registration, which is a registration of 2D fundus image with 3D OCT image. It requires that the 3D OCT image be reduced to 2D image by

z-direction projection [12]. Therefore, the problem of fundus-OCT registration becomes similar as fundus-fundus registration; 3) OCT-OCT registration, which is useful to access temporal changes of retinal layers and enlarge retinal coverage. Among them, OCT-OCT registration is the most challenging one because OCT is a 3D imaging modality and such registration has to be performed in three dimensions.

The two important sources which lead to changes between SD-OCT scans of the same eye are the patient position and the eye motion. The patient position will influence the point of entry of the beam of light emitted by the OCT device into the pupil, which can lead to a deviation in the field of view. Inevitable eye movement during data acquiring process also causes variations. But this kind of variations can be partly corrected by the hardware-based techniques. Therefore, the major deformations in different OCT scans of the same subject are translation, some limited rotation due to eye motion and deformation of the tissues due to expansion and contraction of the vasculature.

Till now, various OCT registration algorithms have been proposed in the literature. The first public method for automated registration of SD-OCT is presented in 2009 [13]. They presented a rigid registration of SD-OCT volumes using 3D SIFT features. Since then, a lot of works which are restricted to the rigid registration [14-18] have been reported. Recently, more and more researchers have realized that it is not enough to describe the deformation of retina using such a low dimensional model and they tried to solve the problem by a deformable registration method. However, considering SD-OCT scans acquire one B-scan at a time, the appropriate way to handle 3D non-rigid registration of the OCT scans is not immediately clear. Some researchers tried to use the non-rigid registration in a single OCT scan to solve segmentation and noise reduction problem. They only use the non-rigid registration in part of the OCT image instead of the whole OCT volume. Zheng et al. [19] used the ANTS Symmetric Normalization (SyN) registration algorithm to aid the OCT retinal layer segmentation and the registration was applied to individual layers instead of the whole OCT image. Zhang et al. reported a two-step image registration method to reduce the speckles in OCT images [20]. The method began with a global rigid transformation and then the local transformation was estimated between successive B-scans by a graph-based algorithm. Cheng et al. proposed a novel speckle reduction method for 3D SD-OCT scans [21]. They globally aligned the consecutive B-scan slices and then locally aligned neighboring A-scans to correct the distortions. This method removed the displacements of a single OCT volume in x and z directions. Since the longitudinal SD-OCT image registration problem is more challenging than that of a single SD-OCT volume, limited works have been reported. The highly-rated deformable registration algorithms for medical images such as SyN [22], DRAMMS [23] are showed to be unreliable when applied to the whole OCT image.

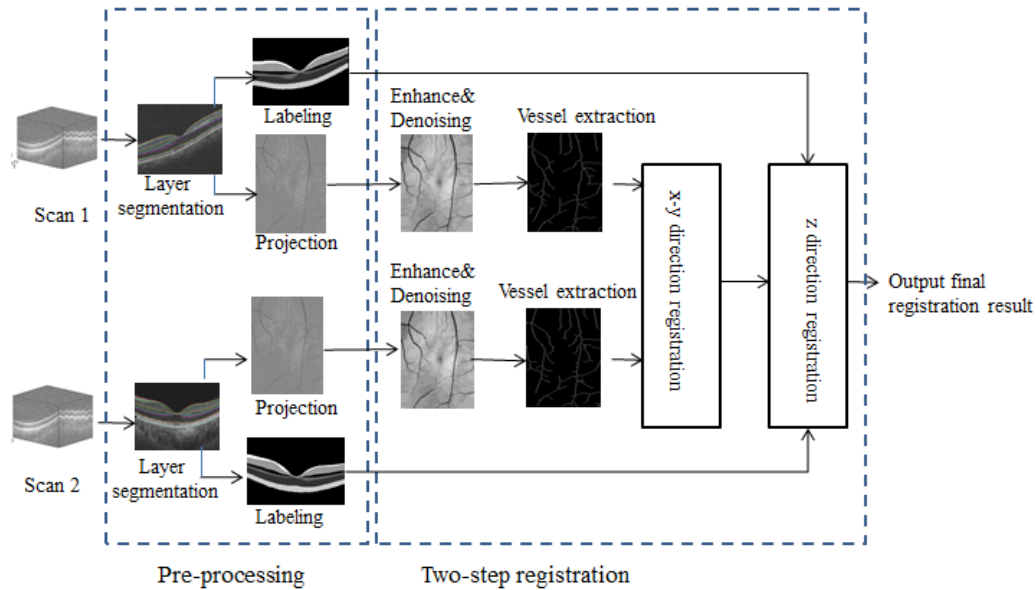


FIGURE 3. Flowchart of the proposed algorithm.

Chen et al. [24] proposed a deformable registration method using A-scan similarity. In their method, the position of retinal fovea which was approximated as the superior point of the thinnest portion of the retina was used for the initial registration and then the retinal layers were aligned by a deformable registration using one-dimensional radial basis function. In our previous work, a two-step registration method using the coherent point drift method followed by non-rigid B-spline-based registration (CPDBS) was introduced [25]. Compared with rigid registration, these retinal OCT deformable registration methods achieve better accuracy while sacrificing computing speed. Since the deformable transformation is a free form mapping at each voxel x , it can be solved by finding a transformation of each voxel to minimize an energy function. Considering the high resolution of OCT data, the energy function would be a very high dimensional function which makes it extremely difficult to find the global optimal solution. The main difficulties are the computation complexity and the local minima problem.

This paper proposes an efficient and accurate registration method for retinal SD-OCT images. To achieve the 3D registration, the x-y direction registration and z direction registration are designed. For x-y direction registration, a vessel skeleton extraction method is applied to generate vessel map, and Speeded-Up Robust Features of the vessel map is used to guide x-y direction registration. For z direction registration, the tissue map is used instead of the intensity image, and a group of A-scans in the neighborhood of the target A-scan are aligned to get the local displacement in z direction. The advantage of this method is that it can achieve good registration accuracy with very low computation complexity. According to our experiments, the

total average computation time is 340 seconds which is very competitive.

The rest of this paper is organized as follows. Section II presents steps of the proposed registration process in detail. Section III discusses the performed experiments and shows the simulation results. Finally, discussions and conclusions are given in Section IV.

II. METHODOLOGY

The proposed method consists of three steps: preprocessing, global x-y direction registration and local z direction registration. The overall flowchart is shown in Fig. 3. In preprocessing step, OCT data are first segmented into 7 surfaces using multi-resolution graph search and the surface segmentation information is then used to calculate the projection image and label the retinal layer tissues. In registration step, a two-step registration method is applied. The vessel information is extracted from the projection images to guide the global x-y direction registration. The labeled tissue maps are used to guide the local z direction registration. The details of each step are discussed in the following parts.

A. PREPROCESSING

In preprocessing step, there are three main tasks: retinal layer segmentation, projection image calculation and retinal layer tissue labeling.

1) *Retinal layer segmentation*: The SD-OCT image is segmented automatically using the multi-layer graph search based method [26], yielding 11 surfaces (10 layers): retinal nerve fiber layer (RNFL), ganglion cell layer (GCL), inner plexiform layer (IPL), inner nuclear layer (INL), outer plexiform layer (OPL), outer nuclear layer and inner

segment layer (ONL+ISL), connecting cilia (CL), outer segment layer (OSL), Verhoeff's membrane (VM), and retinal pigment epithelium (RPE) as shown in Fig. 4. The basic idea of this method is to transform the optimal surface detection problem into computing a minimum s/t cut in an arc-weighted directed graph. The key to transform the optimal surface detection problem into seeking a minimum closed set in a graph is based on the important observation that any feasible surface in a volumetric image uniquely corresponds to a nonempty closed set in a node-weighted directed graphs with the same cost [27, 28]. And the minimum closed set problem is to search for a closed set with the minimum cost, which can be solved by computing a minimum s-t cut. The total cost function is defined in the following way:

$$E = \sum_{v \in S} C_v + \sum_{(p,q) \in N} w_{p,q} (S(p) - S(q)) \quad (1)$$

where S is the desired surface, C_v is an edge-based cost, which is inversely related to the likelihood that the voxel $v \in S$. (p,q) is a pair of neighboring columns and $w_{p,q}$ is a convex function penalizing the desired surface shape change on p,q . The segmented surfaces are then used for producing projection image and labeling retinal layer tissues. Considering some surfaces are very close to each other, we use 7 prominent surfaces among the 11 surfaces to guide the registration. The 7 surfaces are surface1, 2, 4, 5, 6, 7 and 11.

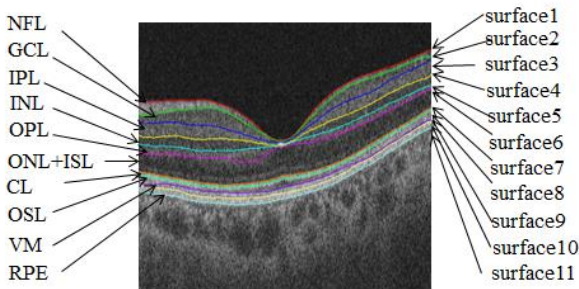


FIGURE 4. Retina surface segmentation illustration.

2) *Projection image calculation*: After retinal layer segmentation, the projection image is calculated. According to the fact that the blood vessels produce a hyper intense area in the inner retina and their shadows produce a hypo intense area in the outer retina, vessel information can be extracted from the projection image of 3D OCT data. To obtain 2D projection image, the intensity values of voxels along each A-scan between the upper surface of RPE layer and Bruch's membrane are averaged.

3) *Retinal layer tissue labeling*: SD-OCT images suffer from serious speckle noise [29-31]. Since traditional intensity based registration methods use image intensities to measure the similarity between the template and the subject image, they tend to be sensitive to deal with such noisy images. To

overcome this problem, we apply a retinal layer tissue labeling method. According to the surface segmentation results, we label the original retinal SD-OCT image into seven prominent tissues including the background, NFL, GCL+IPL, INL, OPL, ONL+ISL and RPE+. As shown in Fig. 5, different intensities represent different tissues of the retina. Using the tissue map instead of the original intensity image in the registration can overcome the speckle noise.

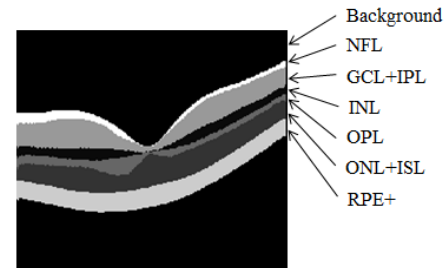


FIGURE 5. Retinal layers after tissue labeling.

B. X-Y DIRECTION REGISTRATION

In our method, the 3D registration is modeled as x-y direction registration and z direction registration. The main target of x-y direction registration is to remove the displacement between the template and the subject image which is caused by different position of the eye. The major deformations that need to be resolved are translation, limited rotation and scaling. To find out the global deformation parameters of the 3D OCT image pair, the vessel maps of their OCT projection images are extracted to guide the registration. However, extracting vessels from OCT projection image is more challenging than from fundus image due to the speckle noise and low resolution [32]. There are several methods for vessel segmentation from the OCT scan. The commonly used methods are vessel detection filter-based method [33], graph theory-based approach [34] and kNN classifier-based method [35]. We adopt the vessel detection filter-based method in our algorithm. Considering the process of achieving retinal OCT images is inevitably disturbed by noises, especially speckle noise, their projection images also suffer from serious speckle noise. In order to obtain a high quality projection image, we adopt Histogram Equalization [36] to adjust the contrast of retinal OCT projection image and improve the visibility of blood vessels. The method can better allocate the intensities by effectively spreading out the most frequent intensity values (Fig. 6(b)). Then we use Wiener filtering to suppress noises. The computational complexity of Wiener filter is much lower compared with other typical digital filters to reduce speckle noise [37]. After that, we get the projection of OCT image with high quality (Fig. 6(c)). As the blood vessels of retinal OCT projection images exhibit a tree bifurcation structure, that is to say the size of the blood vessel changes variously from trunk blood vessel to capillary, it is difficult to detect the micro vessels by using single-scale vessel enhancement filtering. The detection of vessel shadows is divided into two

stages. In the first stage, the multi-scale vessel enhancement filter based on Hessian matrix is applied to detect tubular structures which could be regarded as blood vessels (Fig. 6 (d)). To analyze the local structure of an image I , the Taylor expansion in a neighborhood of pixel A is considered as follows:

$$I(A + \Delta A) \approx I(A) + \Delta A^T \nabla I(A) + \Delta A^T H(A) \Delta A \quad (2)$$

where $\nabla I(A)$ and $H(A)$ are the gradient vector and Hessian matrix of the image computed in pixel A . The detection of vessels can be achieved by analyzing the second order information. The third term in Eq. (2) gives the second order directional derivative. Let λ_1 and λ_2 denote the eigenvalues of the Hessian. For an ideal tubular structure in 2D image, the eigenvalues should satisfy $|\lambda_1| \approx 0$ and $|\lambda_1| \ll |\lambda_2|$ [38]. A vesselness measure function is defined as follows:

$$v_o(\sigma) = \begin{cases} 0 & \lambda_2 > 0 \\ \exp\left(-\frac{R_B^2}{2\beta^2}\right) \left(1 - \exp\left(-\frac{S^2}{2c^2}\right)\right) & \text{otherwise} \end{cases} \quad (3)$$

$$R_B = \frac{|\lambda_1|}{|\lambda_2|} \quad (4)$$

$$S = \|H\|_F = \sqrt{\lambda_1^2 + \lambda_2^2} \quad (5)$$

where R_B is the blob measurement. R_B attains the maximum value for a blob-like structure and equals to 0 when $|\lambda_1| \approx 0$. S is the second order structural measurement.

It is low in the background where no structure is present and becomes larger in the regions with higher contrast compared to the background. The β and c are the thresholds which control the sensitivity of the line filter to the measures R_B and S . In our experiment, β is fixed to 0.5 and c is set to half the value of maximum Hessian norm. The vesselness measure in Eq. (3) is analyzed at different scales. The response will achieve a maximum value at the scale that approximately matches the size of the vessel.

In the second stage, the morphological single-pixel-wide thinning method is used to simplify the vessel structure and to describe the position of the blood vessel clearly. First, the value of the pixels from 220 to 290 in length and from 125 to 150 in width is set to zero to avoid misjudgment of blood vessels due to vasoreflex (Fig. 6 (e)). Then the morphological corrosion is conducted by using the 'disc' structuring element to get rid of noises (Fig. 6 (f)). After that, the thinning method based on mathematical morphology is applied to refine the width of the processed blood vessels into one pixel (Fig. 6 (g)). Finally, biased skeleton of blood vessels are removed when the size of the skeleton is less than a threshold to enhance the accuracy of the vessel detection result. The extracted blood vessel map is shown as Fig. 6 (h).

To ensure fast and accurate registration for vessel maps, Speeded-Up Robust Features (SURF) [39] which can outperform other state-of-the-art local feature detectors in the context of longitudinal registration of retinal images is used [40]. SURF algorithm is invariant to scale and rotation and has low computational complexity. It contains three main steps: interest points determining, direction feature extracting and matching. After applying the SURF method to the extracted blood vessel map, RANSAC approach [41, 42] is used to remove the outliers. Finally, the registration parameter can be obtained. The transformation is therefore described by Eq. (6), where $[x', y']$ is the transformed new position and $[x, y]$ is the original position of the subject image. $a = s \cos \theta$, $b = s \sin \theta$. s is the scale value and θ is the rotation value. t_x and t_y are the value of x-direction translation and y-direction translation, respectively.

$$\begin{bmatrix} x' \\ y' \end{bmatrix} = \begin{bmatrix} a & b \\ -b & a \end{bmatrix} \begin{bmatrix} x \\ y \end{bmatrix} + \begin{bmatrix} t_x \\ t_y \end{bmatrix} \quad (6)$$

The proposed x-y direction registration algorithm can be summarized as follows:

Algorithm 1:

BEGIN

- 1: *Input*: The original projection image;
 - 2: Apply Histogram Equalization and Wiener filtering to the projection image to enhance the image quality and suppress noises;
 - 3: Detect the vessel structure using the multi-scale vessel enhancement filter;
 - 4: Extract the skeleton of vessels using the morphological single-pixel-wide thinning method;
 - 5: Refine the skeleton of vessels and remove the biased skeleton of blood vessels with a threshold-based method;
 - 6: Perform registration using SURF features and remove the outliers using RANSAC;
 - 7: Apply the transformation parameters which are obtained from the registration to the OCT volume to complete the x-y direction registration ;
 - 8: *Output*: The globally registered image;
- END

C. Z DIRECTION REGISTRATION

After x-y direction registration, the x-y direction displacement is corrected. The remaining step to achieve full 3D registration is to find out the displacement along z direction. Instead of simply aligning certain boundary of retina in z direction [43], a two-step z direction registration was performed to overcome the registration error caused by the deformation of retinal layers due to disease. We formulate z direction displacement as a sum of axial motion during 3D OCT scanning and inter displacement between the template and subject images, i.e.,

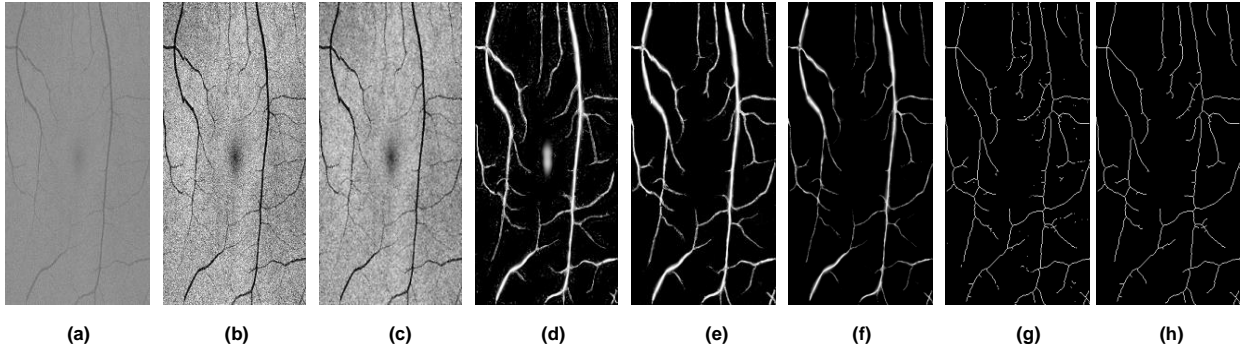


FIGURE 6. (a) Projection image. (b) Enhanced image. (c) Denoised image. (d) Detected blood vessel. (e) Removal of center white spot. (f) Corroded blood vessel. (g) Single-pixel-wide skeleton of vessel. (h) Trimming biased skeleton off.

$$\Delta z = z_{motion} + z_{inter} \quad (7)$$

z_{motion} is caused by the vertical movement of eye and head motion during 3D OCT scanning. In motion distorted data, the position of layers varies greatly in consecutive B-scans which make interpolation and regularization difficult. z_{motion} can be observed in y-z view as shown in Fig. 2(c), where each column corresponds to a B-scan. The template image should be a motion free image. In order to correct axial motion artifacts and provide a more consistent retinal shape for visualization, surface 11 is used as the reference surface for motion correction. The lowest z position of surface 11 is set as the base position l_{base} and the vertical distance $\Delta z_{i,j}$ between surface 11 and the base is calculated to estimate the displacement of each A-scan:

$$\Delta z_{i,j} = l_{base} - l_{11i,j} \quad (8)$$

where $l_{11i,j}$ is the vertical position of surface 11 in each $A_{i,j}$. And then, the OCT volume is flattened by shifting the A-scans down in the z-direction according to the displacement, such that the z positions of surface 11 become the same for all A-scans. Therefore, an axial motion free template image can be obtained. Applying the same process to the subject image can remove the axial motion in the subject image. Considering the serious speckle noise in SD-OCT images, the tissue map is used instead of the original intensity image in the registration to overcome the speckle noise. The local z direction registration is done by applying a vertical displacement on $A_{i,j}$, such that the tissue map difference between the two A-scans in subject and template images is minimized. To increase the robustness, a group of A-scans are used for computing the difference instead of a single A-scan. As illustrated in Fig. 7, $G^T_{i,j}$ and $G^S_{i,j}$ are a group of A-scans centered at $A^T_{i,j}$ and $A^S_{i,j}$ from the k th B-scan B^T_k and B^S_k in the template and the subject images, respectively. Mathematically, the group of A-scans can be written as:

$$G^T_{i,j} = [A^T_{i,j-w}, A^T_{i,j-w+1}, \dots, A^T_{i,j+w-1}, A^T_{i,j+w}] \quad (9)$$

$$G^S_{i,j} = [A^S_{i,j-w}, A^S_{i,j-w+1}, \dots, A^S_{i,j+w-1}, A^S_{i,j+w}] \quad (10)$$

In this paper, we search for the vertical displacement by minimizing the difference between $G^T_{i,j}$ and $G^S_{i,j}$:

$$\min_{\Delta z} \sum_{x,z} |G^S_{i,j}(x, z + \Delta z) - G^T_{i,j}(x, z)| \quad (11)$$

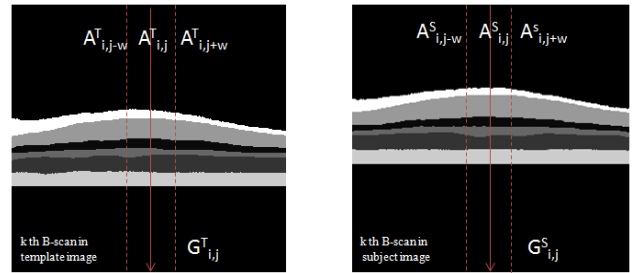


FIGURE 7. Illustration of z direction registration. $A^S_{i,j}$ is aligned with $A^T_{i,j}$ according to the similarity of $G^S_{i,j}$ and $G^T_{i,j}$.

The proposed z direction registration algorithm can be summarized as follows:

Algorithm II:

-
- BEGIN
- 1: *Input:* The x-y direction registered retinal OCT image;
 - 2: Correct axial motion distortions to get axial motion free image;
 - 3: For each A-scan in the template image and the subject image $A^T_{i,j}$ and $A^S_{i,j}$, define a group of A-scans $G^T_{i,j}$ and $G^S_{i,j}$ as in Eq.(9) and Eq.(10);
 - 4: Search for the z direction displacement by minimizing the tissue map difference between $G^T_{i,j}$ and $G^S_{i,j}$;
 - 5: Apply the z direction displacement to the x-y direction registered OCT image to achieve the 3D registration ;
 - 6: *Output:* The final registered image;
-
- END

III. EXPERIMENT AND RESULTS

A. EXPERIMENT DATA AND EVALUATIONS METRICS

To evaluate the performance of the proposed method, macula-centered SD-OCT scans were acquired using Topcon DRI OCT-1 scanner. All the scans were acquired with 256 B-scans, each B-scan having 512 A-scans with 992 pixels per A-scan. The image resolution is $11.72 \times 2.62 \times 23.44 \text{ um}^3$. The dataset includes 45 retinal OCT scans from 15 subjects, with each subject having 3 longitudinal scans. This study was carried out following the principles of the Declaration of Helsinki and approved by the volunteers and patients for publication. The OCT scan from time point 1 was selected as the template. Scans from other time points were registered to the selected template. The proposed method was applied to the longitudinal data of the same subject and the experiment was repeated to all the other subjects from the dataset. Quantitative evaluation is important to justify the advantages of the proposed method. To quantitatively assess the accuracy of the registration algorithm, the Dice overlap ratio and the average surface error which are typically used as the quantitative performance metrics in the OCT registration were calculated. The Dice overlap ratio for each layer between the template and the registered OCT images was calculated as follows:

$$d_k = \frac{2|T_k \cap S_k|}{|T_k| + |S_k|} \quad (12)$$

where d_k is the voxel-wise overlap ratio for retinal layer k ; T_k and S_k are the set of voxels labeled as layer k in the template and the warped subjects. The overlap ratio takes the values between 0 and 1.0. d_k of 1.0 corresponds to full overlap between T_k and S_k , while d_k of 0 corresponds to none overlap. Higher value of d_k shows better registration accuracy. The average surface error which measures the average absolute A-scan distance between each boundary surface in the template and the registered OCT images was also computed. The smaller the average surface error values are, the better registration performance has been achieved.

B. PERFORMANCE EVALUATIONS

To evaluate the performance of the proposed algorithm, three different experiments were performed.

1) *Evaluation of projection image enhancement and denoising*: The x-y direction registration method which is presented in this paper relies on the detection and extraction of the blood vessel points. Extracting vessels from OCT projection images is more challenging than from fundus images due to the speckle noise and low resolution. To enhance the image quality and suppress noises, Histogram equalization (HE) and Wiener filtering (WF) were applied to the projection image. The results are demonstrated in Fig.6. The proposed method is also compared with some other

image enhancement and denoising methods including gray scale transformation method (GST), anisotropic diffusion method (AD) and so on. The blood vessel detection results with different preprocessing methods are shown in Fig.8. From Fig.8, it can be observed that after preprocessing the detected blood vessels are clearer. Although the image enhancement methods enhanced the vessel information, it also enhanced the noises (Fig. 8 (b) and (c)). With the help of denoising methods, the influence of noise can be reduced (Fig. 8 (d) - (g)). The results of Fig. 8 show that use the Histogram equalization and Wiener filtering method as the preprocessing method can achieve the best vessel detection result among all the methods.

2) *Evaluation of x-y direction registration and z direction registration*: After x-y registration, the displacement along x-y direction which is caused by the different position of eyes during the scan process can be corrected. Fig. 9 demonstrates the x-y direction registration using SURF. SURF descriptors are designed to be robust against imaging artifacts and distortions. And they were proved to be more reliable than the bifurcation and cross-over points which are commonly used as landmark points for retinal image registration [36]. By applying x-y direction registration, the original misaligned vessels in Fig. 9 (d) are better aligned in Fig. 9 (e). In addition to the registration performance revealed by the real data, we use the simulated deformations to validate the accuracy of x-y direction registration. The simulated data was created as follows. The projection image of OCT scan from time point 1 in our test dataset was selected as the template. Projection images from other time points were simulated by applying translation, rotation, scaling or a combination of them under the guidance of ophthalmologists. With the known transformation, it is easy to detect the correspondence points in the subject OCT projection image and the template OCT projection image. Suppose the correspondence position for $[x, y]$ in the subject OCT projection image is $[x_r, y_r]$. By applying the proposed x-y direction registration method, $[x, y]$ in the subject OCT projection image can be transformed to the new position $[x', y']$. The pixels are said to be accurately registered if

$$\|(x' - x_r) + (y' - y_r)\|_2 \leq 2 \quad (13)$$

The worst and the best registration results of the simulated data are presented in Fig. 10. The worst registration result is due to the large rotation degree. However it rarely happens in real data. To measure the registration accuracy, we selected several pixels on the vessel skeletons of the vessel map as the key pixels. Suppose the number of the key pixels is N . If the number of the accurately registered pixels is M among the selected pixels, we then can calculate the ratio of M and N to measure the accuracy of the proposed x-y direction registration method. The results are reported in Table I.

Although x-y direction registration corrected the misaligned vessels, the axial motion during 3D OCT

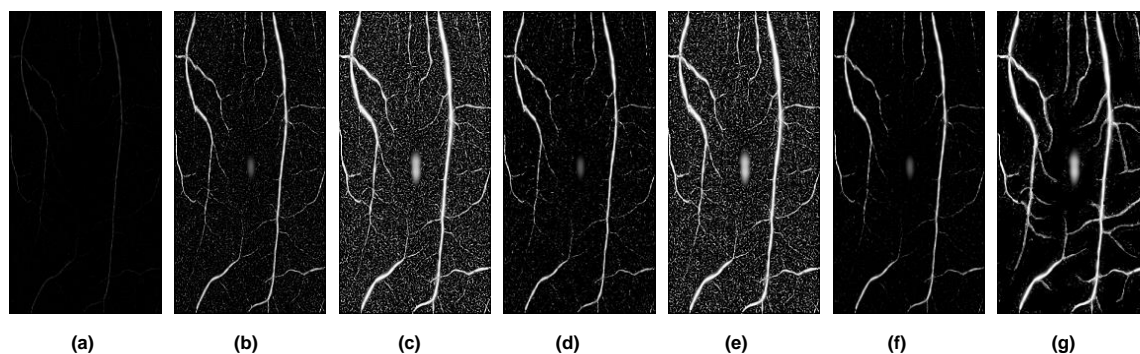


FIGURE 8. Blood vessel detection results with different preprocessing methods (a) No preprocessing. (b) Gray scale transformation (GST). (c) Histogram equalization (HE). (d) Gray scale transformation and anisotropic diffusion (GST & AD). (e) Histogram equalization and anisotropic diffusion (HE & AD). (f) Gray scale transformation and Wiener filtering (GST & WF). (g) Histogram equalization and Wiener filtering (HE & WF).

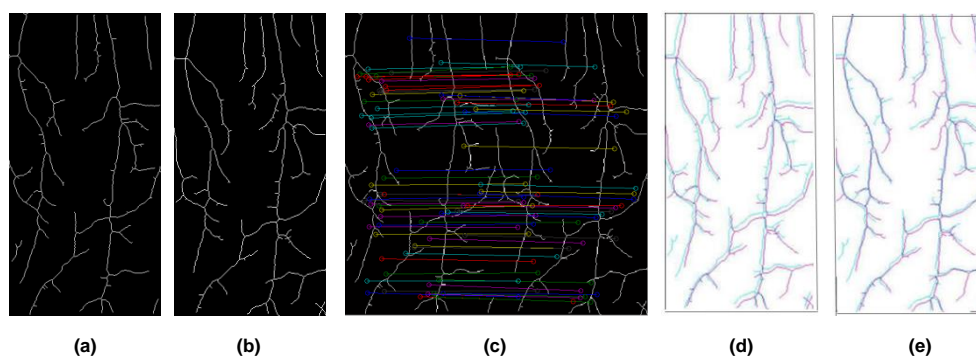


FIGURE 9. Illustration of vessel map registration for the real data. (a) Template vessel map. (b) Subject vessel map. (c) Matching points. (d) Vessel map overlap before registration. (e) Vessel map overlap after registration. The background color is removed in (d) and (e). The vessel skeletons of the template image are set to green and the vessel skeletons of the subject image are set to red for better view.

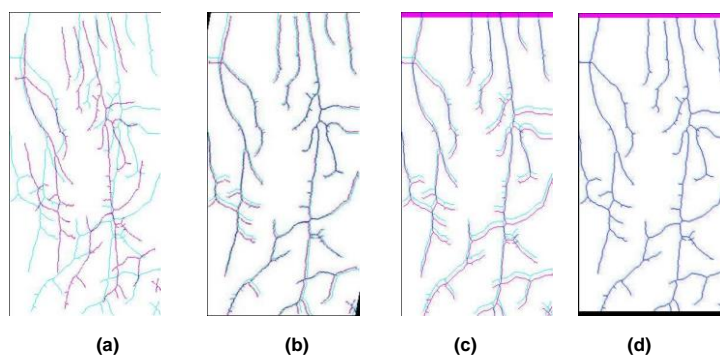


FIGURE 10. Illustration of vessel map registration for the simulated data. (a) (c) Vessel map overlap before registration. (b) (d) Vessel map overlap after registration. The vessel skeletons of the template image are set to blue and the vessel skeletons of the subject image are set to red for better view.

scanning and z direction displacement between the template image and the subject image still exist. Therefore, the z direction registration is quite necessary. We should note that the z direction registration will only change the z position but not the x-y position of an A-scan. Since the main task of z direction registration is to remove the axial motion of OCT scans, we can compare the average surface error to evaluate its performance. The results are summarized in the last column of Table III. It can be observed that after z direction registration the average surface error is obviously reduced which indicates the surfaces of the subject image were well aligned to the template image.

3) *Comparison with other registration methods:* To demonstrate the excellent performance of our algorithm, the proposed method was compared with other typical registration methods including the rigid registration, the highly ranked non-rigid registration algorithm for general medical image registration HAMMER [44] and our previously proposed CPDBS deformable registration method especially designed for OCT images [25]. Fig. 11 demonstrates the registration results by using these different methods for visual comparison. In Fig.11, the first row corresponds to the template image and the subject image. The second row to the fifth row correspond to the registration

results and the checkerboard images by using the rigid registration, HAMMER registration, CPDBS registration and the proposed registration method, respectively.

The experiment results show that the checkerboard image of the rigid registration has many discontinuities. It demonstrates that the rigid registration is not enough to describe the deformation of retina. The registration results of HAMMER show that directly applying HAMMER to the 3D OCT volume will lead to relatively poor performance.

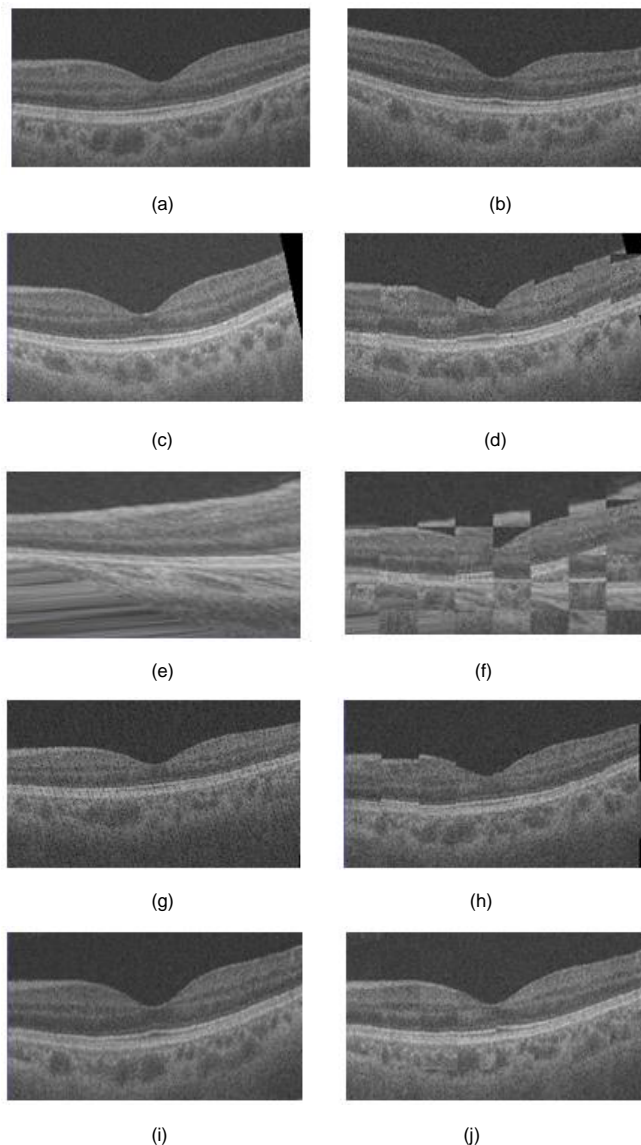


FIGURE 11. An example of registration result by using different registration methods. (a) Temple image; (b) Subject image; (c) Registration result by rigid registration; (d) Checkerboard image of rigid method; (e) Registration result by HAMMER registration; (f) Checkerboard image of HAMMER; (g) Registration result by CPDBS registration; (h) Checkerboard image of CPDBS; (i) Registration result by proposed method; (j) Checkerboard image of proposed method.

This is because HAMMER is initially designed for brain image registration and it does not consider the characteristic of retinal OCT images. Therefore, the feature vectors used in

HAMMER cannot correctly distinguish the retinal structures. CPDBS registration method is especially designed for retinal SD-OCT images. Its registration result shows better performance than the rigid registration and the HAMMER non-rigid registration method. However, the checkerboard image still has some discontinuities which demonstrate that some regions are not well aligned. The main reason is that CPDBS registration method relies on intensity similarity to match the correspondences. However, SD-OCT images suffer from serious speckle noises. The normal intensity based registration methods tend to be more sensitive to the noises during the registration process when the intensity contrast is low. Although the B-spline transform used in CPDBS method can better describe the deformation of retina than the rigid registration, directly using the B-spline transform without considering the geometrical characteristic of OCT images may suffer from the local minima and lead to correspondence mis-matching. Among all the methods, the proposed algorithm shows the best performance. The checkerboard image is smooth which demonstrates that the subject image is well aligned to the template image. This is due to our two innovations. 1) In our method, the 3D registration is modeled as a two-step registration. Since a single A-scan is acquired at a time, voxels have strong correlations along A-scans. Therefore, each A-scan is considered as a base deformable unit and the voxel transformation is not allowed across different A-scans. Therefore, the mis-matching across different A-scans is avoided. 2) The tissue map is used instead of the intensity image in the registration to reduce the negative effect of the speckle noises. Therefore, the registration accuracy is improved.

Table II reports the Dice overlap ratios of each retinal layer by using the above mentioned different registration methods. The overall Dice overlap ratios of six retinal layers is 0.86 by using the proposed registration method and it is higher compared with that of the other registration approaches. We further examined the statistical significance of the improvement of our method via the paired t-tests. Compared with the other registration approaches, our method can achieve statistical significant improvements (p -value < 0.05) in the Dice overlap ratio consistently. Table III reports the average surface error by using the different registration methods. The overall average surface error is 10.2 μ m by using the proposed registration method and it is smaller compared with that of the other registration approaches. The results of the paired t-tests also shows that our method can achieve statistical significant improvements (p -value < 0.05) in the overall average surface errors consistently.

4) *Computation Complexity*: The proposed registration algorithm was implemented in Matlab and tested on a PC with Intel(R) Core(TM) i7-47903.6GHz CPU and 8GB RAM. The average running time of the proposed algorithm is about 340 seconds. The segmentation step, x-y direction registration step and z direction registration step takes

235 seconds, 65 seconds and 40 seconds, respectively. For comparison, the CPDBS method requires 10hours for one registration. Although HAMMER method uses hierarchical attribute matching mechanism to speed up the registration process, it still requires 1 hour to finish one registration.

TABLE I
EVALUATION OF X-Y DIRECTION REGISTRATION

Simulated Data	Accuracy
Translation only	100%
Rotation only	90%
Scaling only	92%
Combination	87%

TABLE II
DICE OVERLAP RATIOS OF 6 RETINAL LAYERS

Layer	Rigid	HAMMER	CPDBS	Proposed method
RNFL	0.67	0.48	0.72	0.81
GCL+IPL	0.82	0.52	0.8	0.89
INL	0.55	0.33	0.76	0.86
OPL	0.68	0.4	0.77	0.79
ONL+ISL	0.8	0.36	0.8	0.9
RPE	0.74	0.43	0.79	0.92
AVG	0.71	0.42	0.77	0.86

TABLE III
AVERAGE SURFACE ERROR (UM)

Surface	Rigid	HAMMER	CPDBS	Proposed method
Surface1	24.5	36.3	16.8	13.5
Surface2	30.2	38.1	18.7	13.8
Surface3	22.6	43.2	20	7
Surface4	26.4	42.5	20.8	7.3
Surface5	23.8	41.8	21.6	14.2
Surface6	25.7	43.1	21.4	7.7
Surface7	23.2	38.6	22.8	7.9
AVG	25.2	40.5	20.3	10.2

C. APPLICATIONS

To show the applications of the proposed registration algorithm, two examples are given in this section

1) *Application in predicting growth of choroid neovascularization*: The first application is using the registration method to help the growth prediction of choroid neovascularization (CNV). CNV is a kind of pathology from the choroid. It is caused by new blood vessels growing in the choroid. CNV-related disease is one important cause of visual disability. As so far, its pathogenesis is still not clear. A standard and effective treatment for CNV is to inject anti-vascular endothelial growth factor (anti-VEGF) agents into the eye to suppress further blood vessel growth. However, such treatment requires frequent re-treatments. Therefore, treatment planning is essential to ensure the efficacy while

reducing the risk. Predicting the growth of CNV based on 3D longitudinal OCT images can greatly help to make the treatment plan. However, since longitudinal OCT images are collected from different times, different positions of eye during the scanning will cause displacements of the retina in OCT images. Such displacements severely affect the accuracy of prediction. Therefore, to guarantee the prediction accuracy and observe the change of lesion area at the same position, registration process is necessary. First, the image registration was conducted on the longitudinal OCT images. In the registration process, since segmenting the layers in CNV data is more challenging than in normal data, the graph search method was first applied to obtain a rough segmentation results. For the data with poor segmentation, we modified the local segmentation results manually under the guidance of an experienced ophthalmologist.

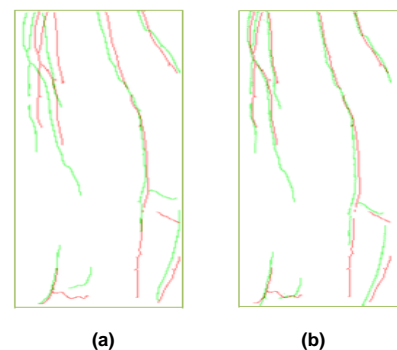


FIGURE 12. Example of registered vessel images. (a) Vessel map overlap before registration. (b) Vessel map overlap after registration. The vessel skeletons of the template image are set to green and the vessel skeletons of the subject image are set to red for better view.

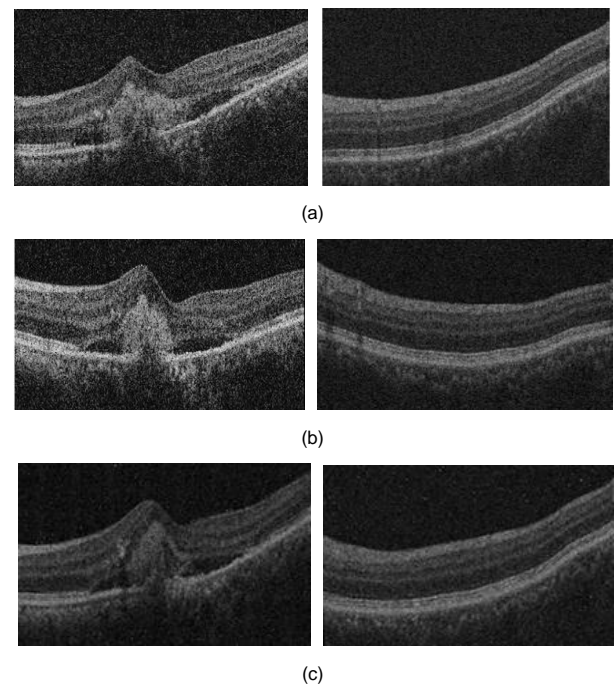


FIGURE 13. Examples of the registered B-scans. First column is the B-scan in CNV region. Second column is the B-scan far away from CNV region. (a) Template image; (b) Subject image; (c) Registration result.

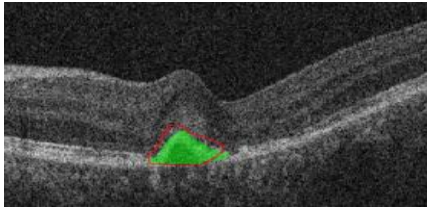


FIGURE 14. An example of CNV prediction result.

Ten pairs of registration were done with CNV data containing $512 \times 128 \times 1024$ voxels and with a resolution of $11.74 \times 1.96 \times 47.24 \text{ } \mu\text{m}^3$. Examples of registered vessel images and registered B-scans are demonstrated in Fig. 12 and Fig. 13. The registration results show that by using the proposed z direction registration method, the average dice overlap ratio can achieve 79%, which is 5% higher than simply aligning the RPE surface in z direction. After registration, reaction diffusion model was applied to predict the CNV growth in 3D OCT images. Fig. 14 shows an example of the result for CNV growth prediction. The green area is the manually segmented CNV result as the ground truth. The red line overlaid on the original image is CNV prediction result. The result has a good prediction in the size and location of the future CNV region.

This method can also be used to guide the treatment planning in clinical practice. Fig. 15 shows the CNV growth measurement at the first three months for the treatment group and the reference group. In the treatment group, anti-VEGF medicine was injected and the disease area decreased obviously. In the reference group, without injecting anti-VEGF medicine, the disease became worse. It can be observed that anti-VEGF medicine can suppress further blood vessel growth and prevent disease progression effectively.

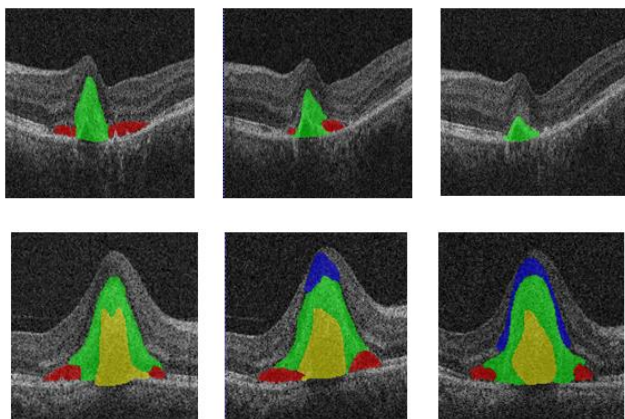


FIGURE 15. CNV growth measurement at the first three months. (a) Treatment group. (b) Reference group. Green, red, yellow and blue area in a B-scan represent CNV area, sub-retinal fluid, pigment epithelial detachment and cystoid edema, respectively.

2) *Application in reducing speckle noise:* In the second example, we show the application of registration to reduce speckle noise. Speckle noise is problematic in OCT images.

It inherently exists in OCT and degrades the image quality. A raw OCT image usually has very poor quality due to the speckle noise. Speckle noise not only affects visual diagnosis, but also increases the challenges in automatic image analysis. Therefore, speckle noise reduction is important. The common approach to improve the OCT image quality is to calculate the average image through overlapping scans. The data to be averaged should be acquired from the same position. However, in practice, slight position changes always happen during scanning due to the movement of the beam and the sample. Therefore, registration is important to overcome the mis-alignment. In our experiment, using the SD-OCT image from time point 1 as the template image, other longitudinal images were registered to the template image. After registration, corresponding B-scan from the longitudinal images are added and averaged to get the clean image.

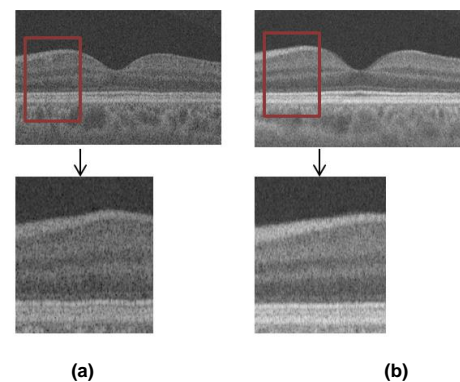


FIGURE 16. Speckle noise reduction by using registration. (a) Original B-scan. (b) The same B-scan after speckle noise reduction.

As shown in Fig. 16, after registration and averaging, the speckle noise is reduced and the quality of OCT image is improved. As we do not have the ground truth image for comparison, traditional measurement such as peak signal to noise ratio cannot be computed here. In this experiment, since we only have three longitudinal scans for each subject in our dataset, three longitudinal scans were used for averaging. It should be noted that with more overlapping scans, the image quality can be further improved.

IV. CONCLUSION AND DISCUSSION

In this paper, we proposed a novel algorithm for 3D retinal OCT image registration by modeling the problem as a two-step registration problem including x-y direction registration and z direction registration. In the proposed method, the vessel maps are extracted from the projection image of 3D OCT scans and x-y direction displacement is estimated by matching Speeded-Up Robust Features of the vessel maps. Then, using the tissue map instead of the original intensity image, a group of A-scans in the neighborhood of the target A-scan are aligned to get the local displacement in z direction. The proposed method was tested on longitudinal data with three time points on fifteen eyes. Experimental results proved the feasibility and accuracy of the proposed method. In the

proposed method, since z direction registration is guided by the layer segmentation results, the segmentation accuracy will directly affect the accuracy of the registration. Nowadays, many new retinal layer segmentation algorithms have been proposed. One class is graph-based methods. For example, our latest work proposed NNCGS segmentation method [45] which achieves better layer segmentation accuracy in OCT images with choroidal neovascularization. However, the computation complexity of this method is very high and the running time is twice longer than that of the method we used in this paper. Therefore, when dealing with large data set, the segmentation efficiency is low. Another popular class is deep learning-based segmentation methods. For example, the latest published work CE-Net [46] showed excellent segmentation results. Even though deep learning-based method always shows better segmentation accuracy than traditional method, it has some shortcomings. The training process is time consuming and a large number of training samples are required. The segmentation method used in this paper is not the most accurate one but has the following advantages: 1) it is guaranteed to find the three-dimensionally optimal solution with respect to the cost function; 2) it can deal with both normal and diseased retinal OCT image; 3) it can obtain high accuracy with low computation complexity. Although, the multi-resolution graph search segmentation results are generally found accurate and robust in our experiment, automatic accurate surface segmentation is not easy for pathological region with dramatic change in the layer structure. Furthermore, since the retinal layers in OCT image are plate-like structure, neighbor A-scans are very similar to each other. To avoid mis-matching across different A-scans, only limited deformations are considered in x-y direction and each A-scan is fixed as a base deformable unit. However, higher dimensional transformation models with the aid of well designed features can better describe the deformation of retina. Future work will focus on improving the method to automatic process serious diseased retinal OCT images and designing higher dimensional transformation models to better describe the deformation of retina.

REFERENCES

- [1] J. G. Fujimoto, W. Drexler, J. S. Schuman, and C. K. Hitzenberger, "Optical Coherence Tomography (OCT) in ophthalmology: introduction," *Optics Express*, vol.17, no. 5, pp. 3978-3979, 2009.
- [2] M. R. Hee, J. A. Izatt, E. A. Swanson, D. Huang, J. S. Schuman, C. P. Lin, C. A. Puliafito, and J. G. Fujimoto, "Optical coherence tomography of the human retina," *Archives Ophthalmology*, vol.113, no.3, pp. 325-332, Apr. 1995.
- [3] M. Wojtkowski, A. Kowalczyk, R. Leitgeb, et al, "Full range complex spectral optical coherence tomography technique in eye imaging," *Optics Letters*, vol. 27, no. 16, pp. 1415-1417, Sep. 2002.
- [4] G. J. Jaffe and J. Caprioli, "Optical coherence tomography to detect and manage retinal disease and glaucoma," *American Journal of Ophthalmology*, vol.137, no.1, pp.156-169, Feb. 2004.

- [5] M. D. Abramoff, M. K. Garvin, and M. Sonka, "Retinal Imaging and Image Analysis," *IEEE Reviews in Biomedical Engineering*, vol. 3, pp. 169-208, 2010.
- [6] A. Sotiras, C. Davatzikos, and N. Paragios. "Deformable medical image registration: a survey," *IEEE Transactions on Medical Imaging*, vol. 32, no.7, pp. 1153-1190, May 2013.
- [7] D. L. Hill, P. G. Batchelor, M. Holden, et al, "Medical image registration," *Physics in Medicine & Biology*, vol.31, no.4, pp.1-45, Jan. 2008.
- [8] T. M. Jørgensen, J. Thomsen, U. Christensen, W. Soliman, and B. Sander, "Enhancing the signal-to-noise ratio in ophthalmic optical coherence tomography by image registration—method and clinical examples," *J. Biomed. Opt.* vol.12, no.4, pp.041208-041208, July 2007.
- [9] K. K. Brock, M. B. Sharpe, L. A. Dawson, S. M. Kim, and D. A. Jaffray, "Accuracy of finite element model-based multi-organ deformable image registration," *Med. Phys.* vol.32, no.6, pp.1647-1659, July 2005.
- [10] E. A. Van, W. J. Niessen, S. Klein, et al., "Multi-feature-based plaque characterization in ex vivo MRI trained by registration to 3D histology," *Physics in Medicine & Biology*, vol.57, no.1, pp.241-256, Dec. 2012.
- [11] R. Magjarevic, G. Troglio, A. Nappo, J. A. Benediktsson, G. Moser, S.B. Serpico, and E. Stefansson, Automatic change detection of retinal images vol. 25/11, pp. 281-284, 2009 [Online]. Available: http://dx.doi.org/10.1007/978-3-642-03891-4_75
- [12] J. A. Lee, J. Cheng, G. Xu, et al., "Registration of color and OCT fundus image using low-dimensional step pattern analysis," in *Proc. MICCAI*, 2015, pp. 214-221.
- [13] M. Niemeijer et al. "Registration of 3D spectral OCT volumes using 3D SIFT feature point matching," in *Proc. SPIE*, USA, 2009, 725911.
- [14] D.Alonso-Caneiro, S. A. Read, M. J. Collins, "Speckle reduction in optical coherence tomography imaging by affine-motion image registration," *Journal of Biomedical Optics*, vol.16, no.11, pp. 116027, Nov. 2011.
- [15] G. J. Ughi et al., "Automatic three-dimensional registration of intravascular optical coherence tomography images," *Journal of Biomedical Optics*, vol.17, no.2, pp.026005, Feb.2012.
- [16] Y. M. Liew, R. A. McLaughlin, F. M. Wood, and D. D. Sampson, "Motion correction of in vivo three-dimensional optical coherence tomography of human skin using a fiducial marker," *Biomedical Optics Express*, vol.3, no.8, pp.1774-1786, Aug. 2012.
- [17] J. Xu, H. Ishikawa, G. Wollstein, L. Kagemann, and J. S. Schuman, "Alignment of 3-D optical coherence tomography scans to correct eye movement using a particle filtering," *IEEE Transactions on Medical Imaging*, vol.31, no.7, pp.1337-1345, Jan. 2012.
- [18] T. Ronchetti et al., "Detecting Early Choroidal Changes Using Piecewise Rigid Image Registration and Eye-Shape Adherent Regularization," in *Proc. International Workshop on Ophthalmic Medical Image Analysis*, USA, 2017, pp. 159-167.
- [19] Y. Zheng, R. Xiao, Y. Wang, and J. C. Gee, "A generative model for OCT retinal layer segmentation by integrating graph-based multi-surface searching and image registration," in *Proc. MICCAI*, 2013, pp. 428-435.
- [20] H. Zhang, Z. Li, X. Wang, and X. Zhang, "Speckle reduction in optical coherence tomography by two-step image registration," *Journal of Biomedical Optics*, vol.20, no.3, pp. 36013, Mar. 2015.
- [21] J. Cheng, D. Tao, Y. Quan, D. W. K. Wong, G. C. M. Cheung, M. Akiba and J. Liu, "Speckle Reduction in 3D Optical Coherence Tomography of Retina by A-Scan Reconstruction," *IEEE Trans on Medical Imaging*, vol. 35, no. 10, pp. 2270-2279, 2016.
- [22] B. B. Avants, C. L. Epstein, M. Grossman, and J. C. Gee, "Symmetric diffeomorphic image registration with crosscorrelation: Evaluating automated labeling of elderly and neurodegenerative brain," *Medical Image Analysis*. vol. 12. pp.26-41, 2008.
- [23] Y. Ou, A. Sotiras, N. Paragios, and C.Davatzikos, "DRAMMS: Deformable registration via attribute matching and mutual-saliency weighting," *Medical Image Analysis*1, vol.5, no.4, pp.622-639, 2011.
- [24] M. Chen , A. Lang, H. S. Ying, P. A. Calabresi, J. L. Prince, and A. Carass, "Analysis of macular OCT images using deformable registration," *Biomedical Optics Express* , vol. 5, no. 7, pp. 2196-2214, July 2014.

- [25] Q. Wei, et al. "Nonrigid registration of 3D longitudinal optical coherence tomography volumes with choroidal neovascularization," in *Proc. SPIE, USA*, 2017, 101330X.
- [26] F. Shi, X. Chen, H. Zhao, et al. "Automated 3-D Retinal Layer Segmentation of Macular Optical Coherence Tomography Images with Serous Pigment Epithelial Detachments," *IEEE Trans. Med. Imag.*, vol.34, no.2, pp. 441-452, Sep. 2015.
- [27] K. Li, X. Wu, D. Z. Chen, and M. Sonka, "Optimal Surface Segmentation in Volumetric Images—A Graph-Theoretic Approach," *IEEE Transactions on Pattern Analysis & Machine Intelligence*, vol.28, no.1, pp. 119-134, Feb. 2006.
- [28] X. Chen and L. Pan, "A Survey of Graph Cuts/Graph Search based Medical Image Segmentation," *IEEE Reviews in Biomedical Engineering*, vol.11, pp.112-124, Jan. 2018.
- [29] Y. Ma, X. Chen, W. Zhu, X. Cheng, D. Xiang and F. Shi, "Speckle noise reduction in optical coherence tomography images based on edge-sensitive cGAN," *Biomedical Optics Express*, vol.9, no.11, pp. 5129-5146, Nov. 2018
- [30] M. Szkulmowski, I. Gorczynska, D. Szigal, et al., "Efficient reduction of speckle noise in Optical Coherence Tomography," *Optics Express*, vol.20, no.2, pp.1337-1359, Jan. 2012.
- [31] A. Wong, A. Mishra, K. Bizheva, et al., "General Bayesian estimation for speckle noise reduction in optical coherence tomography retinal imagery," *Optics Express*, vol.18, no.8, pp. 8338-52, Apr. 2010.
- [32] A. Lang, et al, "Combined registration and motion correction of longitudinal retinal OCT data," in *Proc. SPIE Medical Imaging*, San Diego, CA, 2016, vol.9784, p.97840X.
- [33] J. Wu, et al., "Stable registration of pathological 3D-OCT scans using retinal vessels," in *Proc. OMI*, Boston, MA, 2014, pp. 1-8.
- [34] A. Stankiewicz, et al., "Volumetric segmentation of human eye blood vessels based on OCT images," in *Proc. EUSIPCO*, Greece, 2017, pp. 36-40.
- [35] M. Niemeijer, et al., "Vessel segmentation in 3D spectral OCT scans of the retina," in *Proc. SPIE*, San Diego, CA, 2008, vol.6914, p.69141R.
- [36] S. M. Pizer, E. P. Amburn, J. D. Austin, et al., "Adaptive Histogram Equalization and Its Variations," *Computer Vision Graphics and Image Processing*, vol.39, no.3, pp.355-368, Sep.1987.
- [37] A. Ozcan, et al. "Speckle reduction in optical coherence tomography images using digital filtering," *Journal of the Optical Society of America A Optics Image Science & Vision*, vol.24, no.7, pp. 1901-1910, 2007.
- [38] A. Frangi, W. J. Niessen, K. L. Vincken, M. A. Viergever, "Multiscale vessel enhancement filtering," in *Proc. MICCAI*, 1998, pp. 130-137.
- [39] Bay, Herbert, T. Tuytelaars, and L. V. Gool, "SURF: Speeded Up Robust Features," *Computer Vision & Image Understanding*, vol.110, no.3, pp. 404-417, Jan. 2006.
- [40] S. K. Saha, D. Xiao, S. Frost, et al. "Performance Evaluation of State-of-the-Art Local Feature Detectors and Descriptors in the Context of Longitudinal Registration of Retinal Images," *Journal of Medical Systems*, vol.42, no.4, pp.57, 2018.
- [41] Chum, Ondřej, J. Matas, and J. Kittler. "Locally Optimized RANSAC," in *Proc.DAGM*, Magdeburg, Germany, 2003, pp.236-243.
- [42] W. Zhang and J. Kosecka, "Generalized RANSAC Framework for Relaxed Correspondence Problems," in *International Symposium on 3D Data Proceeding*, Chapel Hill, North Carolina, USA, 2006, pp.1-7.
- [43] A. Lang, et al, "Longitudinal graph-based segmentation of macular OCT using fundus alignment," in *Proc. SPIE*, Orlando, Florida, 2015, vol.9413, p. 94130M.
- [44] D. Shen, and C. Davatzikos, "HAMMER: Hierarchical Attribute Matching Mechanism for Elastic Registration," *IEEE Transactions on Medical Imaging*, vol. 21, no. 11, pp. 1421-1439, Nov. 2002.
- [45] D. Xiang, H. Tian, X. Yang, F. Sh, W. Zhu, H. Chen and X. Chen, "Automatic Segmentation of Retinal Layer in OCT Images with Choroidal Neovascularization," *IEEE Transactions on Image Processing*, vol. 27, no.12, pp. 5880-5891, Dec. 2018.
- [46] Z. Gu, J. Cheng, H. Fu, K. Zhou, H. Hao, Y. Zhao, T. Zhang, S. Gao and J. Liu, "CE-Net: Context Encoder Network for 2D Medical Image Segmentation," *IEEE Transactions on Medical Imaging*, in press, 2019.